SECTION 3

CONTROL ALGORITHM DEVELOPMENT

The control algorithms developed for the full-scale test were based on classical linear optimal control laws previously discussed by Chung et al. (1988,1989) and Reinhorn et al. (1989). However, unlike in the laboratory, the use of displacement measurements as feedback state variables in conventional control design is not feasible in the field. Under the constraint that only three velocity sensors are available, two alternative control strategies were developed. They are (1) velocity feedback with observer which provides full-dimensional state feedback with the aid of a state-estimator and (2) three-velocity feedback which treats the full-state as an equivalent reduced-order system. These control algorithms are described below following a brief summary of the classical linear optimal control theory.

3.1 Basic Considerations

The classical linear optimal closed-loop control algorithm which is the basis of the control design is reviewed herein. The equation of motion of a discrete-parameter structure, under earthquake excitation $x_o(t)$ and active control force which is expressed in terms of actuator displacement $u(t)$, is described in the state-space representation as:

$$\dot{\underset{\sim}{z}}(t) = \underset{\sim}{A}\,\underset{\sim}{z}(t) + \underset{\sim}{b}\,u(t) + \underset{\sim}{w}\,x_o(t) \qquad (1)$$

where

$$\underset{\sim}{z}(t) = \begin{bmatrix} \underset{\sim}{x}(t) \\ \dot{\underset{\sim}{x}}(t) \end{bmatrix}, \underset{\sim}{A} = \begin{bmatrix} 0 & I \\ -\underset{\sim}{M}^{-1}\underset{\sim}{K} & -\underset{\sim}{M}^{-1}\underset{\sim}{C}_d \end{bmatrix}, \underset{\sim}{b} = \begin{bmatrix} 0 \\ -\underset{\sim}{M}^{-1}\underset{\sim}{b}_1 \end{bmatrix}, \underset{\sim}{w} = \begin{bmatrix} 0 \\ \underset{\sim}{w}_1 \end{bmatrix} \qquad (2)$$

where $\underset{\sim}{z}(t)$ is the state vector of order $2n$ consisting of vectors $\underset{\sim}{x}(t)$ and $\underset{\sim}{x}(t)$

which are the relative displacement and relative velocity vectors of order n, respectively, n being the number of degrees of freedom (DOF) of the structure ($n = 6$ in the present case); $u(t)$ is the actuator displacement that characterizes the control force. Matrices $\underset{\sim}{M}$, $\underset{\sim}{C}_d$ and $\underset{\sim}{K}$ are the mass, damping and stiffness matrices, respectively, which

can be estimated through identification tests. Vector $\underset{\sim}{b}_1$ is the control force location

vector of order n, whose elements are $2k_c \cos \alpha$ for the corresponding floor where the active braces are attached and zero otherwise, k_c being the stiffness of the active brace and α the brace inclination angle from the horizontal, $\underset{\sim}{w}_1$ is a vector of order

with all elements equal to -1 , , indicating the contribution of the ground acceleration.

Based on the classical quadratic performance criterion, $u(t)$ is found by minimizing the integral:

$$J = \frac{1}{2}\int_o^{t_f} \left[\underset{\sim}{z}^T(t)\underset{\sim}{Q}\underset{\sim}{z}(t) + ru^2(t) \right] dt \qquad (3)$$

for the duration t_f of ground excitation. In Eq. (3), $\underset{\sim}{Q}$ is a positive semi-definite weighting matrix for the response and r is a positive weighting factor for the control.

In the present case, matrix $\underset{\sim}{Q}$ is chosen to be:

$$\underset{\sim}{Q} = \begin{bmatrix} K & 0 \\ 0 & 0 \end{bmatrix} \tag{4}$$

so that the first term in Eq. (3) characterizes the potential energy of the structure, and

$$r = 2\beta k_c \tag{5}$$

such that the second term in Eq. (3) characterizes the control energy. β is a control parameter which determines the relative importance between safety and economy; $\beta = \infty$ represents the uncontrolled case. It is noted from the above derivation that β is the only parameter that needs to be specified in the control design.

Under linear feedback control, $u(t)$ is obtained to be linearly related to the state vector $\underset{\sim}{z}(t)$ as (Sage 1977, Chung et al. 1988,1989):

$$u(t) = \underset{\sim}{G}\ \underset{\sim}{z}(t) = r^{-1}\underset{\sim}{b}^T \underset{\sim}{P}\ \underset{\sim}{z}(t) \tag{6}$$

where $\underset{\sim}{G}$ is the feedback gain of order $2n$ and $\underset{\sim}{P}$ is obtained from the approximated time invariant Ricatti matrix question:

$$\underset{\sim}{P}\ \underset{\sim}{A} + \underset{\sim}{A}^T \underset{\sim}{P} - \underset{\sim}{P}\ \underset{\sim}{b}\, r^{-1}\underset{\sim}{b}^T \underset{\sim}{P} + \underset{\sim}{Q} = \underset{\sim}{0} \tag{7}$$

It can be seen from the above that information of all state variables, i.e., displacements and velocities, is required in order to calculate the feedback control force. This requirement, however, is impractical in field applications either because all the state variables are not

accessible for direct measurement or because the available sensing devices are limited. In the present full-scale structural test, only three velocity sensors are provided in each of the principle directions which necessitates modifications.

3.2 Velocity Feedback with Observer

Suppose the state variables of a dynamic system are not fully accessible. In order to apply the state feedback strategy, a state observer can be used if the system is completely observable (Chen 1984).

Consider a dynamical system whose state equation is given by Eq. (1) and the associated output or observation equation is expressed as:

$$\underset{\sim}{y}(t) = \underset{\sim}{C}\,\underset{\sim}{z}(t) \tag{8}$$

where $\underset{\sim}{y}(t)$ is the observed vector of order $m(m \leq 2n)$ and $\underset{\sim}{C}$ is the $mx2n$

measurement matrix. Assuming that $\hat{\underset{\sim}{z}}(t)$ is an estimator of $\underset{\sim}{z}(t)$, then the state observer equation can be written as (Chen 1984, Soong 1989):

$$\dot{\hat{\underset{\sim}{z}}}(t) = \underset{\sim}{A}\,\hat{\underset{\sim}{z}}(t) + \underset{\sim}{b}\,u(t) + \underset{\sim}{w}\,\dot{x}_o(t) + \underset{\sim}{L}\left(\underset{\sim}{y}(t) - \underset{\sim}{C}\,\hat{\underset{\sim}{z}}(t)\right) \tag{9}$$

where $\underset{\sim}{L}$ is the $2nxm$ observer matrix.

Let $\tilde{\underset{\sim}{z}}(t)$, be the error between the actual state vector $\underset{\sim}{z}(t)$, and the estimated state

vector $\hat{\underset{\sim}{z}}(t)$, i.e:

$$\underset{\sim}{\tilde{z}}(t) = \underset{\sim}{z}(t) - \underset{\sim}{\hat{z}}(t) \tag{10}$$

Substituting Eqs. (1) and (9) into Eq. (10), one obtains:

$$\dot{\underset{\sim}{\tilde{z}}}(t) = \left(A - \underset{\sim}{L}\,\underset{\sim}{C}\right)\underset{\sim}{\tilde{z}}(t) \tag{11}$$

It is seen from Eq. (11) that, if the observer matrix $\underset{\sim}{L}$ is properly selected so that the eigenvalues of matrix $\left(A - \underset{\sim}{L}\,\underset{\sim}{C}\right)$ have negative real parts smaller than $-\sigma$, then all elements of the error vector $\underset{\sim}{\tilde{z}}(t)$ will die out at rates faster than $e^{-\sigma t}$. Consequently,

even if there is large error between $\underset{\sim}{\hat{z}}(t_o)$ and $\underset{\sim}{z}(t_o)$ at initial time t_o, the vector $\underset{\sim}{\hat{z}}(t)$ will approach $\underset{\sim}{z}(t)$ rapidly.

Once the full-dimensional state vector is established, the state feedback control can be accomplished by substituting the observed state $\underset{\sim}{\hat{z}}(t)$ for the real state $\underset{\sim}{z}(t)$ in Eq. (6), giving:

$$u(t) = -r^{-1}\,\underset{\sim}{b}^{T}\,\underset{\sim}{P}\,\underset{\sim}{\hat{z}}(t) \tag{12}$$

In an effort to reduce on-line computation, an approximation is introduced in solving Eq. (11) by using finite differences. Equation (9) then becomes a difference equation in the discrete-time form:

$$\dot{\underset{\sim}{z}}(t) = \left[\underset{\sim}{I} - \left(\underset{\sim}{A} - \underset{\sim}{L}\,\underset{\sim}{C} + \underset{\sim}{b}\,\underset{\sim}{G}\right)\Delta t\right]^{-1}\left[\hat{\underset{\sim}{z}}(t-\Delta t) + \underset{\sim}{w}\,\Delta t\,\ddot{x}_o(t) + \underset{\sim}{L}\,\Delta t\,\underset{\sim}{y}(t)\right] \qquad (13)$$

It is noted that, in order to predict the state vector at time instant t, , the knowledge of ground acceleration $\ddot{x}_o$ at time t and the estimated state vector at the previous time step are required along with the available output measurements. As a consequence, an increase in on-line computation is inevitable with a potential increase in time delay, which is critical in real time control.

In the present study, two velocity transducers located at the first and third floors are selected for output measurements of the system. To illustrate the effectiveness of the proposed control algorithm, a series of numerical simulations were performed with various β values using the 32% El Centro earthquake as input. The observer matrix is $\underset{\sim}{L}$ determined in a way that the poles of matrix $\left(\underset{\sim}{A} - \underset{\sim}{L}\,\underset{\sim}{C}\right)$ are assigned to be three times of those of matrix $\underset{\sim}{A}$ so that the error term will diminish rapidly. The correlation between the control force requirement with the weighting factor β is shown in Fig. 3.1(a), where the associated control efficiency in terms of reductions in maximum structural relative displacement, maximum absolute acceleration and maximum base shear is given in Fig. 3.1(b). It is seen that, as expected, the smaller the β value, the better the performance. The case of $\beta = 4$ is determined for the design of ABS as will be explained in the next section. As an illustration, time histories of the top floor response and base shear corresponding to $\beta = 4$ are shown in Fig. 3.2. The associated control force requirement is shown in Fig. 3.3(a).

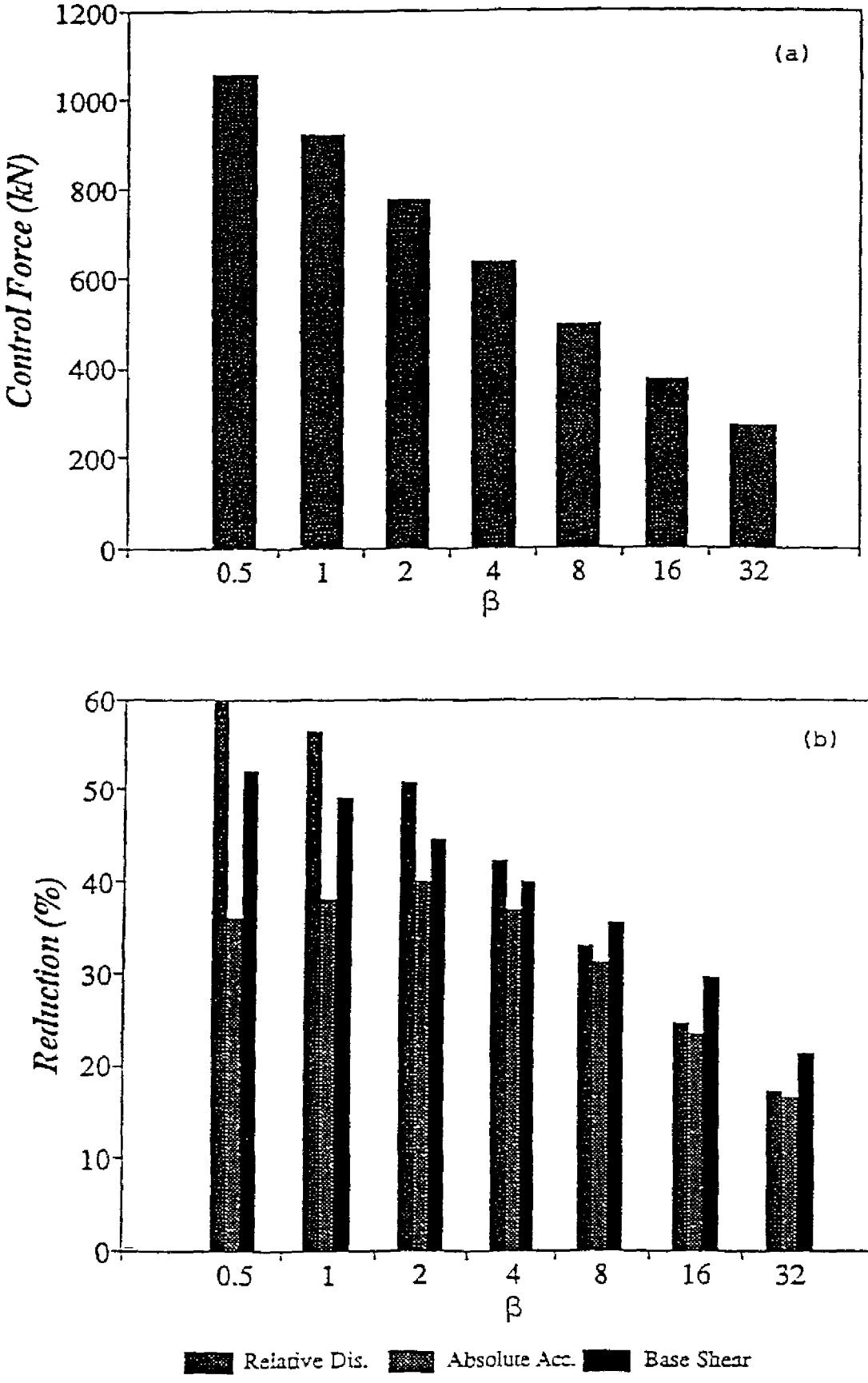

Fig. 3.1 Control Parameters as Functions of (β)

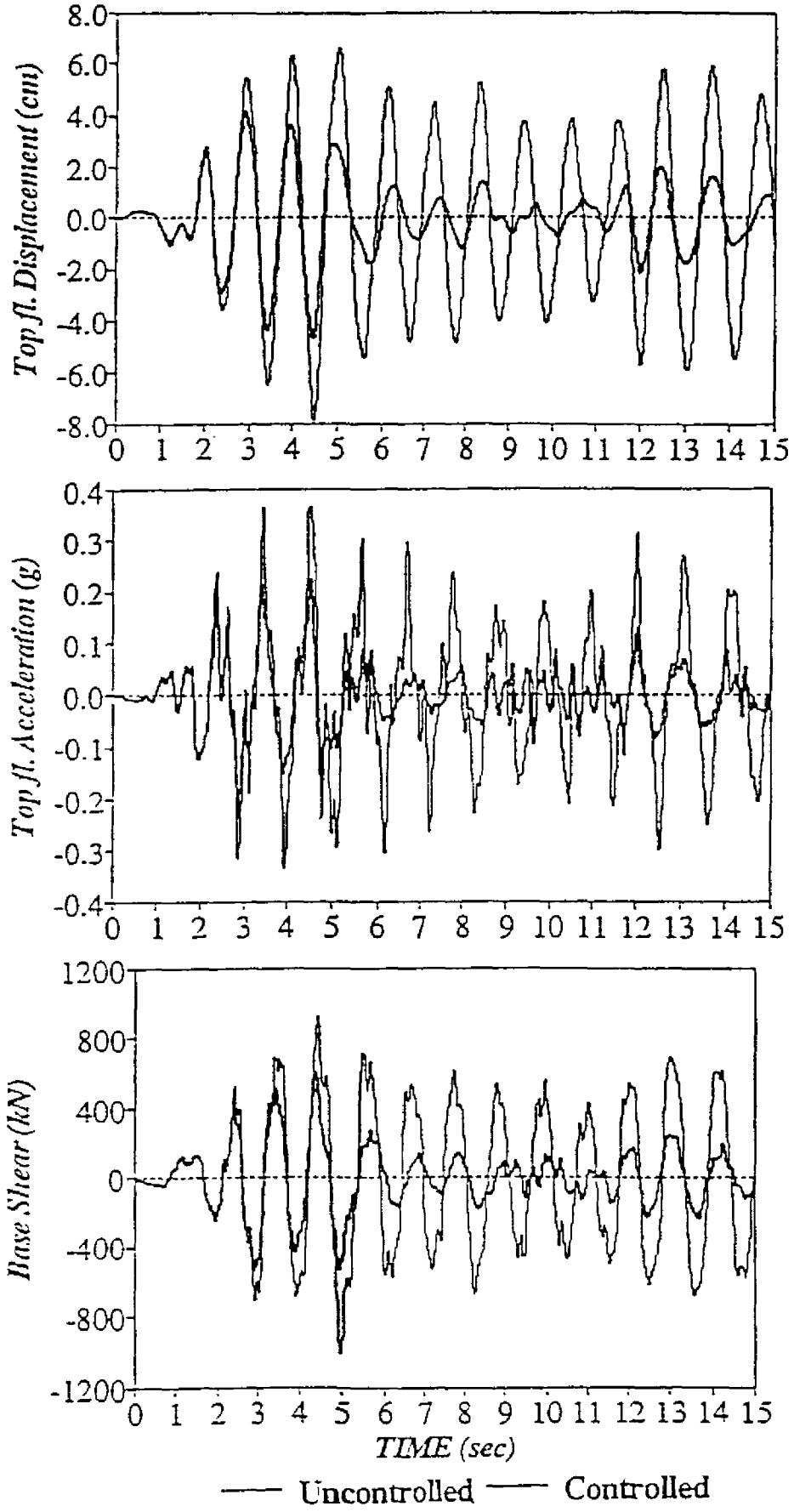

Fig. 3.2 Structural Response under 32% El Centro Earthquake (β = 4)

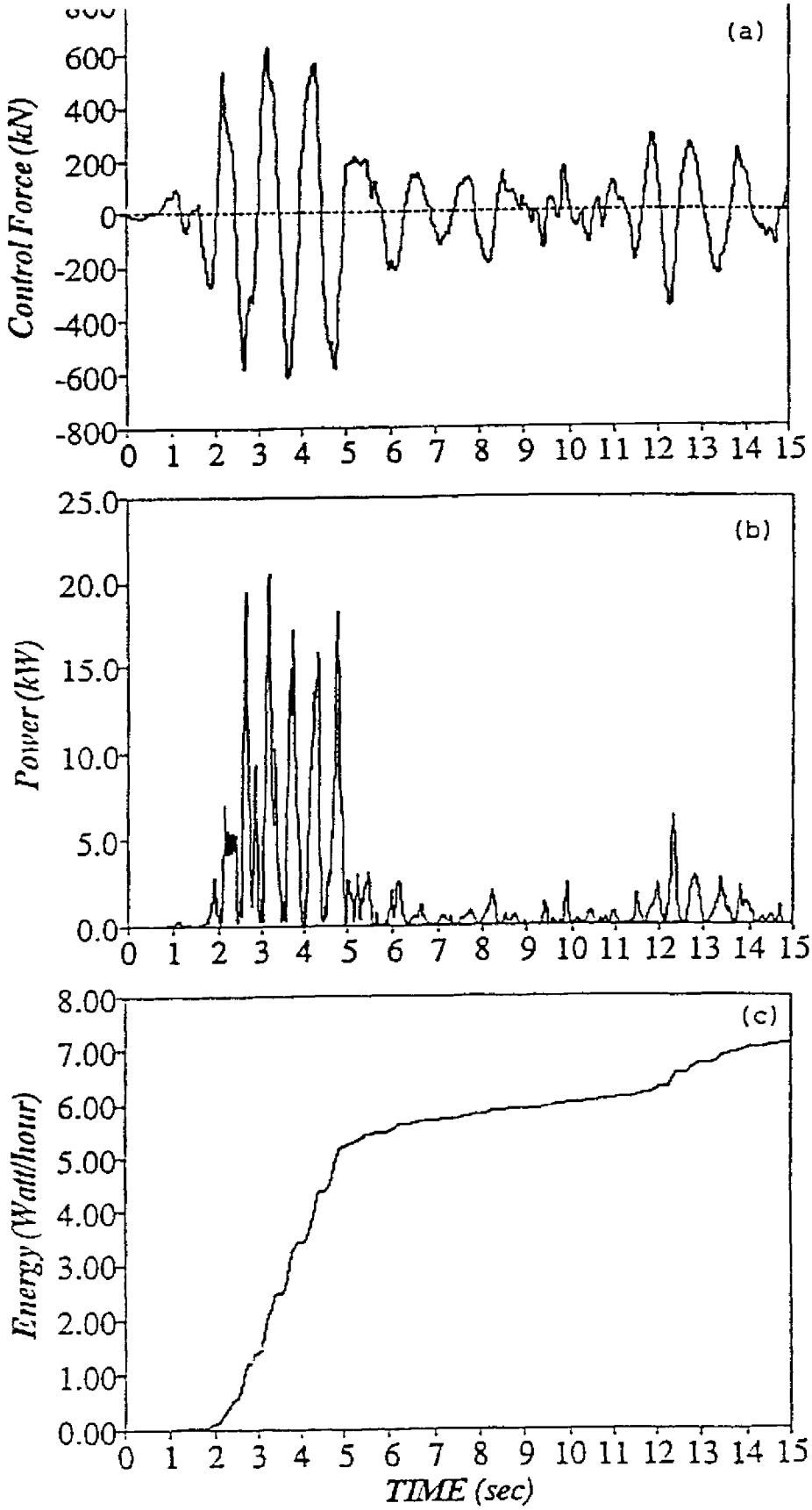

Fig. 3.3 Control Requirements under 32% El Centro Earthquake (β = 4)

3.3 Three-Velocity Feedback Control

Since three velocity sensors are available at the first, third and sixth floors, an alternate control design is one using direct three-velocity feedback. In this development, the full-order system is first reduced to a 3-DOF system and the mode shapes of the reduced order system are constructed from the first three modes of the frequency response functions of relevant floors. It is noted that orthogonality between the mode shapes does not hold here because a part of the modal displacement information has been discarded. A mode smoothing procedure to improve the modal orthogonality is therefore conducted for a more comprehensive dynamic analysis whereby the masses are redistributed to three nodal points and the equivalent stiffness and damping matrices are derived, respectively, by pre- and post-multiplying the diagonal generalized stiffness and damping matrices by the inverse modal matrix. Accordingly, the natural frequencies of the reduced order system are close to the first three modes of the full-order system.

The control design is now developed using velocity information only. The effectiveness of this strategy is confirmed by simulation. The difference between the control efficiency of using both displacement and velocity feedback and that of using velocity feedback alone is insignificant as can be seen in the last two columns of Table 3.1. However, it is interesting to see that less control force is required in the velocity feedback case but more power is required.

Control requirements and structural performance using different control strategies are also compared in Table 3.1. While the control algorithm with observer gives the best result as expected, its implementation requires more on-line computation time, as mentioned earlier, implying greater increase in time delay and reduction in control efficiency.

Table 3.1 Performance Comparisons with Different Control Algorithms

Control Algorithm	uncontrolled	Observer Control	Full-state Feedback Based on 3DOF	Velocity Feedback Based on 3DOF
Top fl. Rel. Disp. Maximun (cm) Reduction (%)	7.9769	4.6673 41.5	5.0406 36.8	5.0480 36.7
Top fl. Abs. Acc. Maximun (g's) Reduction (%)	0.3678	0.2340 36.4	0.2555 30.5	0.2576 30.0
Base Shear Maximun (kN) Reduction (%)	1019.7	606.6 40.5	632.7 38.0	650.3 36.2
Control Force (kN)		629.1	565.5	563.4
Power Requirement (kW)		20.47	24.1	28.8

3.4 Time Delay

In real time control, time delay is contributed mostly by signal processing, on-line computation, and control execution using the hydraulic system. These time delays accumulated in the control loop can cause deterioration of control performance or even system instability if they are not properly compensated (Soong 1990).

Time delay can be determined from the phase lag measured between the signal input and signal output for a given system component. In an identification test, the phase lag angle is determined from the imaginary and real parts of the input and output frequency transfer functions. The delay time for each component of the system is in turn determined by:

$$T_d = \frac{\theta}{360 f} \tag{14}$$

where T_d is the time delay in seconds, θ is the phase lag in degrees and f is the frequency in Hertz.

A preliminary assessment of time delay of the hydraulic actuators used in this test was carried out in the laboratory. Using banded white noise as input, the delay time between the command signal and the achieved actuator response was estimated to be about 12 msec. The required on-line computation time was also estimated in a similar manner to be about 14 msec for the observer control algorithm and 5 msec for the three-velocity feedback algorithm.

Among various time delay compensation methods, phase compensation that was first discussed by Roorda (1980) and verified effective in laboratory experiments (Chung et al. 1988, McGreevy et al. 1988 and Chung et al. 1989) is one of the most attractive strategies. This method is adopted in the present study as briefly described below

If the displacement feedback force lags the displacement by τ_x in time while velocity feedback force lags the velocity by τ_x ,their corresponding phase lags for the i-th mode are $\omega_i\tau_x$ and $\omega_i\tau_x$. With the phase shift, the displacement feedback force may be resolved to produce positive active stiffness and negative active damping while the velocity feedback force may be resolved to produce positive active stiffness and positive active damping. Due to the existence of negative active damping, control effects are diminished for the real system as compared to the ideal one. Even worse, time delay will cause instability if the resultant damping force is negative. Since phase lag is proportional to the delay time and modal frequency, the effect of time delay can become serious for higher modes even with small amounts of time delay.

The control force contributed by the i-th mode can be expressed as (Chung et al. 1989):

$$u_i(t) = -g_{1i}\eta_i(t) - g_{2i}\dot{\eta}_i(t) = -g'_{1i}\eta_i(t - \tau_x) - g'_{2i}\dot{\eta}_i(t - \tau_x) \qquad (15)$$

where g'_{1i} and g'_{2i} are the modified displacement and velocity feedback gains, respectively, with time delay compensation. The modified feedback gain factors are determined so that the same control effect can be achieved.

Due to phase shift, the displacement feedback forces contributed by the mode can be resolved into $(g'_{1i}\cos\omega_i\tau_x)\eta_i$ as a displacement component and $(-g'_{1i}\sin\omega_i\tau_x)\eta_i/\omega_i$ as a velocity component. Similarly, the displacement and velocity components of the velocity feedback force contributed by the i-th mode are, respectively, $(g'_{2i}\sin\omega_i\tau_x)\omega_i\eta_i$ and $(g'_{2i}\cos\omega_i\tau_x)\eta_i$. In order to make the real system equivalent to the ideal one, the relationship between feedback gains for the real

system and those for the ideal system can be established such that both systems have the same active stiffness and active damping. Thus, the modified feedback gains are obtained as :

$$[g'_{1i}\ g'_{2i}] = [g_{1i}\ g_{2i}] \begin{bmatrix} \cos\omega_i\tau_x & -(1/w_i)\sin\omega_i\tau_x \\ \omega_i\sin\omega_i\tau_x & \cos w_i\tau_x \end{bmatrix}^{-1} \qquad (16)$$

For multi-degree-of-freedom systems, the control gain correction due to time delay as indicated in Eq. (16) can be applied to each mode in the modal domain and transformed into the physical domain through modal transformation. More detailed derivation can be found in (Reinhorn and Soong et al. 1989).

SECTION 4

DESIGN OF ACTIVE CONTROL

4.1 Design Earthquakes

For design purposes, the peak velocity of the design earthquakes was taken to be 10 cm/sec based on local seismic records over the past seven years (maximum = 9.5 cm/sec). Accordingly, the scaled (32%) El Centro earthquake with 98 cm/sec^2 (0.1 g) peak acceleration was determined as the design earthquake which corresponds to the criterion of 10 cm/sec maximum velocity. Response analyses were also carried out using a series of recorded earthquake time histories to verify the adequacy of the design specifications. Table 4.1 tabulates the earthquakes considered in the verification of the control system with their maximum accelerations scaled to 0.1 g.

4.2 Analysis and Design

4.2.1 Determination of weighting factor β.

A series of numerical simulations with different β values have been presented in the preceding section. While the best reduction in displacement was observed in the case of $\beta = 0.5$, $\beta = 4$ was used for control system design from the practical standpoint since it gave satisfactory structural performance (approximately 40% reduction) while requiring reasonable amount of control force (665 kN), just within the capacity of the selected actuators. The associated maximum actuator displacement and velocity are ($\pm$)0.5 cm and 6.6 cm/sec, respectively, also within the performance limitation of the specified device. The following analysis for design of the power resource is based on this β value.

Table 4.1 Design Earthquakes

Earthquakes	Component	Scale factor	Duration (sec)	Sampling time (sec)
El Centro	NS	0.32	20	0.02
Hachinohe	NS	0.60	20	0.01
Miyagioki		0.68	30	0.01
Taft	N21E	0.715	20	0.02
Mexico	N90W	0.65	100	0.02
Mexico	S00E	1.115	100	0.02
Pacomia Dam	S16E	0.095	20	0.02
Pacomia Dam	S74W	0.104	20	0.02
Tokyo		1.48	10	0.02

4.2.2 Design of passive power resource.

The required flow rate $\dot{q}(t)$ of the hydraulic cylinders can be determined approximately in terms of the piston area A_p and the actuator velocity $u(t)$ as:

$$q(t) = A_p u(t) \tag{17}$$

in which $\dot{u}(t)$ is calculated based on the selected β value and the assumed brace stiffness.

Equation (17) is a first-order approximation in which compressibility of the hydraulic fluid and leakage around the valve and piston are neglected, which is adequate only when the load reaction is small. In general, maximum values are the criteria of design specification. The design capacity of the flow rate, however, is not based on the extreme value; it is rather determined in accordance with the average flow rate from an economic point of view The servo-controlled system pumps the hydraulic oil with a constant speed during the control action. The difference of the oil flow between the required and the supplied is then adjusted through the hydraulic accumulators.

Figure 4.1 illustrates the cumulative flow accumulated during an earthquake, which is obtained by integrating the time history of the flow rate. The slope of this curve represents the instantaneous flow rate required to achieve the control goal. It is observed from interpreting the slope of the curve that system demand is the highest between 2 and 5 seconds and less so over the rest of the time history, a property apparently resulted from the nonstationary nature of the earthquake motion and the control effect contributed in the previous time period. The linear curve represents the cumulative volume of a constant flow which is obtained by minimizing the difference between the demand and supply

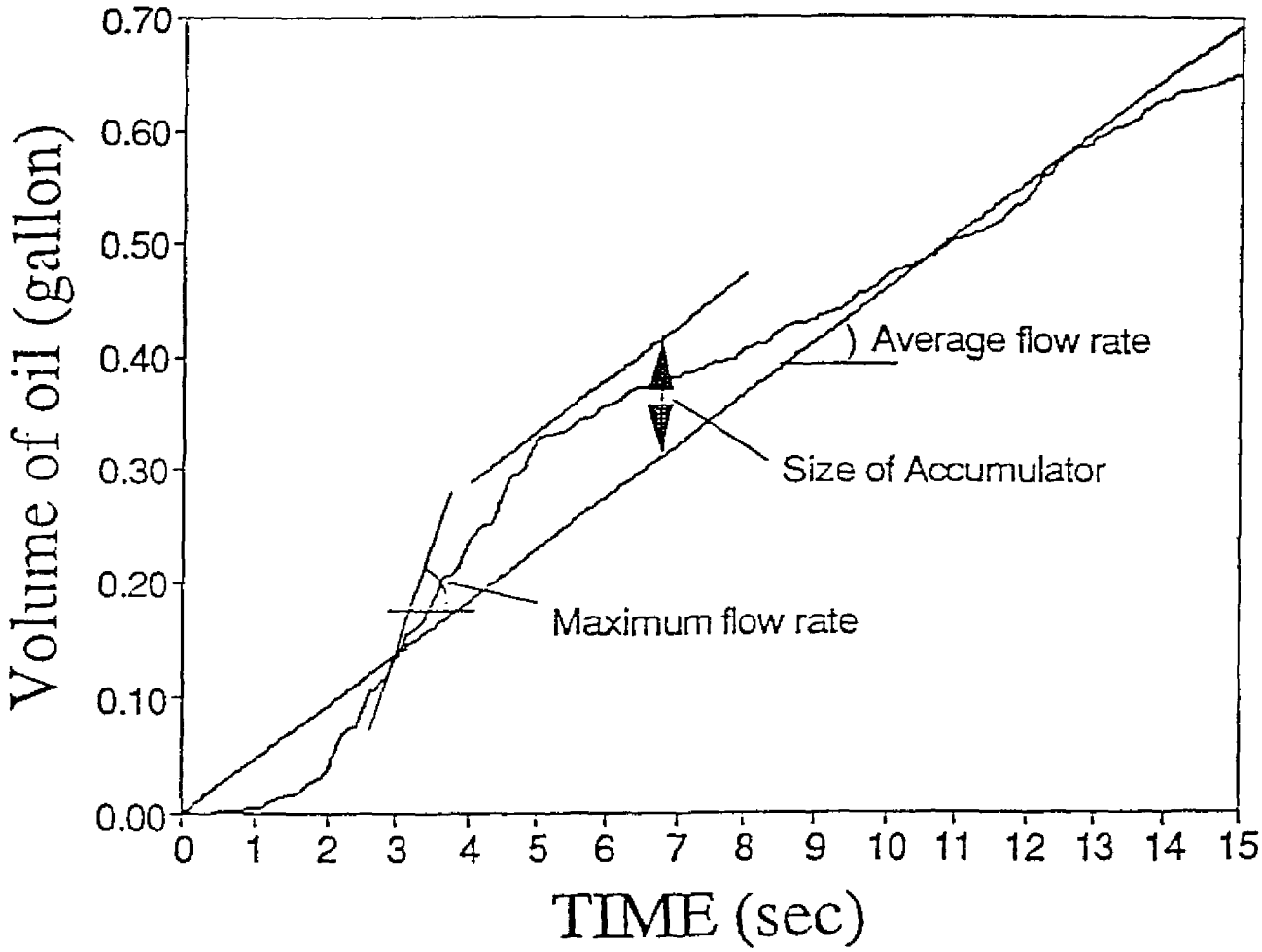

Fig. 4.1 Cumulative Oil Flow During 32% El Centro Earthquake

of oil using the least-square criterion. The largest difference between the cumulative flow and the average flow indicates the minimum volume of the hydraulic accumulator to be considered in design.

A summary of simulated results under representative earthquakes is given in Table 4.2. The ABS design specifications are determined accordingly.

4.3 Verification

From the analytical data shown in Table 4.2, it was found that the design was appropriate for almost all earthquake records used except for the case of Hachinohe earthquake. In that case, it requires a maximum control force of 696.5 kN which is far beyond the design capacity of the system if the same control strategy is to be used. Investigation was made by restricting the output control force within the design capacity of the actuator while using the same feedback gains. Results show less reduction of structural response (about 30% in displacement and 47% otherwise) when the control force is restricted to 333 kN per actuator whereas stability of the mechanical system is preserved.

This situation should also be taken into account in the on-line control practice due to erratic nature of earthquake ground motions.

4.4 Power and Energy

In order to generate the required control forces, large power supply may be required to effectively activate the actuators. Power requirement, $p(t)$, of the hydraulic system can be evaluated in terms of the control force $F(t)$, and actuator velocity $u(t)$ as:

$$p(t) = F(t)u(t) \tag{18}$$

Energy consumption, $E(t)$, can be obtained from:

Table 4.2 Summary of Response Analysis under Design Earthquakes (β = 4)

Earthquakes	Scale factor		Performance indices			Resource requirement / Actuator						
			Top fl disp. (cm)	Top fl. acc. (g)	Base shear (kN)	control Force (kN)	Actuator disp. (cm)	Max. flow rate (gpm)	Ave. flow rate (gpm)	Vol.of accum. (gal.)	Total volume of oil (gal.)	Power (Kw)
El Centro	0.32	Unctrl Ctrl Red.(%)	7.98 4.66 41.6	0.37 0 23 36.5	1018.3 618 0 39.5	313.9	0.51	19.72	2.7	0.11	0.74 in 20 s	20.02
Miyagioki	0 68	Unctrl Ctrl Red.(%)	5.30 3.27 36.4	0.43 0.21 50.7	847 6 547.4 35.8	245.3	0.40	15.24	2.0	0.12	0.71 in 30 s	16.08
Mexico (N90W)	0.65	Unctrl Ctrl Red.(%)	9.70 5.80 40 2	0.32 0.18 44.2	1347.9 877.0 35.0	255.1	0.41	6.21	1.2	0.18	1.33 in 100 s	5.65
Mexico (S00E)	1.115	Unctrl Ctrl Red.(%)	9.95 6.99 29.8	0.34 0.24 30.4	1389.1 1000.6 28.2	323 7	0.53	9.36	1.5	0.34	2.13 in 100 s	10.77
Pacomia Dam (S16E)	0.095	Unctrl Ctrl Red.(%)	5.58 3.90 30.1	0.35 0.17 50.7	741.6 500.3 32.7	255.1	0.42	10.94	2.0	0.06	0.47 in 20 s	10.06
Pacomia Dam (S74W)	0.104	Unctrl Ctrl Red.(%)	4.14 2.68 35.1	0.30 0.14 52.6	606.3 406.1 33.0	176.6	0.29	9.35	2.0	0.055	0.44 in 20 s	4.88
Taft (N21E)	0.715	Unctrl Ctrl Red.(%)	7.64 4.36 42.9	0 63 0.30 53.3	1083.0 535.6 50.5	333.5	0.54	18.29	3.0	0.12	0.96 in 20 s	21.48
Tokyo	1.48	Unctrl Ctrl Red.(%)	4.85 3.73 23.2	0.33 0.26 21.1	623.9 406.1 34.6	333 5	0.54	12.63	2.7	0.07	0.37 in 10 s	21.60
Hachinohe	0.60	Unctrl Ctrl Red.(%)	17.93 9.48 47.1	0.79 0.41 48.6	2731.1 1471.5 46.0	696.5	1.13	26.74	6.0	0.17	1.51 in 20 s	59.02
Hachinohe (limited Ctrl force)	0.60	Unctrl Ctrl Red.(%)	17.93 12.65 29.4	0.79 0.69 12.5	2731.1 1660.8 39.2	333.5	0.54	31.04	4.0	0.17	1.21 in 20 s	55.54

$$E(t) = \int_o^t p(\tau)dr = \int_o^t F(\tau)u(\tau)d\tau \qquad (19)$$

Figures 6(b) and 6(c) illustrate the time histories of power and energy resources required under the 32% El Centro earthquake.